Research Article

# Sustainable Hydrogen Generation through Solid Polymer Fuel Cell Autothermal Reforming for Improved Heat and Power Efficiency

**Hassan Ali Ozgoli**[*] , **Sara Deilami**

School of Engineering, Macquarie University, Sydney, Australia
E-mail: hassanali.ozgoli@mq.edu.au

**Abstract:** This research introduces an innovative integration of a Polymer Electrolyte Membrane Fuel Cell (PEMFC) with a Combined Heat and Power (CHP) system utilizing autothermal reforming (ATR) of natural gas. This novel approach focuses on large-scale industrial applications, addressing scalability and performance optimization, areas previously underexplored. The study conducts a comprehensive parametric analysis of system efficiency, achieving a remarkable 91.3% total efficiency, with 38.1% electrical efficiency and 46.1% thermal efficiency. Economic analysis revealed strong regional differences, with Europe offering the highest Net Present Value (NPV) and a payback period of 4.0 years, while Iran showed a longer payback period of 8.3 years. The system demonstrated adaptability to fluctuating electricity prices, particularly in the U.S. Environmentally, the system achieved a 50% reduction in $CO_2$ emissions and reduced natural gas consumption compared to conventional gas turbines. This innovative study addresses scalability challenges and offers new insights into optimizing PEMFC-CHP systems for sustainable industrial energy generation, contributing to the advancement of clean energy technologies.

*Keywords*: polymer electrolyte membrane fuel cell, combined heat and power, autothermal reforming, energy efficiency, $CO_2$ emissions reduction

## 1. Introduction

The global energy sector is increasingly focused on reducing greenhouse gas emissions and improving energy efficiency, with Combined Heat and Power (CHP) systems emerging as a crucial technology in this transition. CHP systems, which simultaneously generate electricity and thermal energy from a single fuel source, are known for their ability to achieve overall efficiencies of up to 80% or higher, compared to around 50% for conventional power generation methods [1]. This efficiency gain is achieved by capturing and utilizing waste heat that would otherwise be lost, making CHP systems a key component in sustainable energy strategies [2].

Polymer Electrolyte Membrane Fuel Cells (PEMFC) have garnered considerable attention as an effective technology for integration into Combined Heat and Power (CHP) systems due to their high electrical efficiency and adaptability across a broad range of applications. Recent advancements in PEMFC technology have addressed several critical performance and cost challenges, broadening their adoption potential.

Studies have shown that improvements in membrane durability and performance at low relative humidity have extended the operational reliability of PEMFCs under varied environmental conditions. For instance, Shang et al. [3]

demonstrated that a poly (phenylene sulfonic acid)-expanded polytetrafluoroethylene composite membrane enhances PEMFC performance under low-humidity conditions, achieving stable hydration and maintaining high proton conductivity even in dry environments. This advancement is crucial for applications in regions with low ambient humidity, where traditional membranes often suffer from dehydration and reduced efficiency.

Additionally, efforts to reduce the cost of catalysts have made PEMFCs more economically viable. Bayendang et al. [4] reviewed the integration of PEMFCs within Combined Cooling, Heating, and Power (CCHP) systems and highlighted the significance of developing lower-cost catalyst materials, which contribute to reduced overall system costs and improved economic feasibility. Their study indicates that cost-effective catalysts could lead to a reduction in capital expenditures by up to 15%, enhancing the appeal of PEMFC technology in commercial and industrial applications.

Furthermore, integrating PEMFCs with electrolyzers for energy storage and generation has been explored for boosting system efficiency and economic return. Escobar-Yonoff et al. [5] assessed the performance and economic potential of combining PEMFCs with PEM electrolyzers, finding that such systems can achieve efficiencies exceeding 70% while reducing operational costs through renewable energy integration. This setup not only enhances energy output but also enables flexible operation to meet dynamic power demands. These advancements—improved membrane resilience, cost-effective catalyst development, and innovative system integration—collectively enhance the performance, reliability, and economic viability of PEMFCs, supporting their broader implementation in CHP and CCHP systems.

Recent advancements in PEMFC technology have focused on reducing costs and improving the durability of the proton exchange membranes, which are critical to the operation of these systems. For instance, new materials and fabrication methods are being developed to reduce the reliance on expensive platinum catalysts, which has been a significant cost driver in PEMFC systems. Studies have shown that by optimizing the membrane electrode assembly, it is possible to reduce the cost of PEMFC systems to below $1000 per kW, making them more competitive with traditional energy generation technologies [6, 7].

Autothermal reforming (ATR) of natural gas has emerged as a promising method for on-site hydrogen production, essential for the operation of PEMFCs in CHP systems. ATR combines partial oxidation and steam reforming processes to efficiently convert natural gas into hydrogen, significantly reducing carbon emissions compared to conventional methods. The integration of ATR with PEMFCs in CHP systems has been shown to enhance overall system efficiency, with studies reporting reductions in carbon emissions by up to 50% in industrial applications [8, 9].

However, despite these technological advancements, the practical implementation of PEMFC-CHP systems remains underexplored, particularly in large-scale industrial contexts. Previous research, such as that by Pilatowsky et al. [10] and Hwang and Zou [11], has demonstrated efficiency gains of up to 30% in small-scale applications, but these studies often lack comprehensive economic analyses that consider the scalability and long-term viability of these systems in broader industrial applications.

This study aims to address these gaps by providing a detailed evaluation of the technical and economic feasibility of a PEMFC-CHP system that incorporates autothermal reforming of natural gas. Unlike previous research, which has often been limited in scope, this study offers a holistic analysis that includes system design, performance assessment, cost analysis, and environmental impact evaluation. By focusing on large-scale industrial applications, this research seeks to provide new insights into the practicality and scalability of PEMFC-CHP systems, addressing the limitations identified in earlier studies.

The novelty of this research lies in its comprehensive approach, combining both technical and economic analyses to offer a more complete understanding of the potential of PEMFC-CHP systems in industrial settings. The findings are expected to contribute significantly to the ongoing development of PEMFC technology and support its broader adoption across various sectors, particularly in industries where energy demands are substantial, and efficiency gains are most needed.

## 2. System configuration

### 2.1 *Solid Polymer Fuel Cell (SPFC)*

SPFCs also known as PEMFCs, are a type of fuel cell that uses a solid polymer as electrolyte. These fuel cells operate at relatively low temperatures (typically around 60–100 °C) and are known for their high-power density, rapid startup, and potential for use in various applications, including portable power, transportation, and stationary power generation. SPFCs are widely used in applications where clean, efficient, and quiet power sources are required. Recent advances have focused on improving membrane materials, enhancing catalyst performance, and developing better water and thermal management systems. Nanostructured catalysts and alternative ionomer membranes are some of the cutting-edge developments aimed at reducing costs and increasing the efficiency and durability of SPFCs [12].

Recent advancements in polymer electrolyte membranes have further enhanced the efficiency and durability of SPFCs, focusing on improving proton conductivity and reducing costs. Alternative ionomer membranes are increasingly developed to achieve higher performance under various environmental conditions. For example, recent research on polymer electrolyte membranes incorporated with 2D silica nanosheets demonstrates enhanced stability and proton conductivity at high temperatures, which is essential for long-term fuel cell durability [13]. Furthermore, polybenzimidazole-based membranes are emerging as strong candidates to overcome the limitations of traditional Nafion membranes by offering improved performance in high-temperature environments and under low-humidity conditions [14]. Additionally, stainless-steel bipolar plate coatings have been developed to mitigate corrosion in aggressive environments, further extending the lifespan and operational stability of proton-exchange membrane fuel cells [15].

The structure of an SPFC is composed of several key components: the anode, cathode, solid polymer electrolyte membrane, and bipolar plates. The solid polymer electrolyte, usually made of Nafion, is the core of the cell, allowing protons to pass through while acting as a barrier to electrons and gases.

The performance of SPFCs is governed by the thermodynamics of the reactions and the electrochemical behavior of the cell components. The cell voltage (V) in an ideal scenario is given by the Nernst equation:

$$V = V_0 - \frac{RT}{2F} Ln \left( \frac{p_{H_2} \cdot \sqrt{p_{O_2}}}{p_{H_2O}} \right) \tag{1}$$

where $V_0$ is the standard electrode potential, R is the universal gas constant, T is the temperature in Kelvin, F is Faraday's constant, $pH_2$, $pO_2$, and $pH_2O$ are the partial pressures of hydrogen, oxygen, and water, respectively.

In real-world applications, the actual voltage output of an SPFC is lower than the theoretical value due to losses or overpotentials associated with activation, ohmic, and mass transport limitations.

This loss is associated with the energy barrier that must be overcome for the electrochemical reactions to occur at the electrodes. It is described by the Tafel equation [12]:

$$\eta_a = \frac{RT}{\alpha F} Ln \left( \frac{i}{i_0} \right) \tag{2}$$

where $\eta_a$ is the activation overpotential, $\alpha$ is the charge transfer coefficient, i is the current density, $i_0$ is the exchange current density.

Ohmic losses are due to the resistance to the flow of ions through the electrolyte and electrons through the electrodes and external circuit. These losses are directly proportional to the current density:

$$\eta_{ohm} = i \cdot R_{ohm}$$

where $R_{ohm}$ is the total ohmic resistance of the cell.

Mass transport limitations arise when the reactants are not supplied to the reaction sites at a sufficient rate, leading to concentration gradients. This is typically modeled using the following relation:

$$\eta_{mt} = -\frac{RT}{nF} Ln \left(1 - \frac{i}{i_L}\right) \tag{3}$$

where $i_L$ is the limiting current density.

One of the critical challenges in SPFC operation is water management. The membrane must remain hydrated to maintain proton conductivity, but excessive water can lead to flooding, particularly at the cathode, which reduces the active surface area available for the reaction. Water management strategies include controlling the humidity of the inlet gases and designing the cell architecture to optimize water distribution. Thermal management is also essential, as the operation of SPFCs generates heat. If not adequately managed, this heat can lead to membrane dehydration or hot spots, which degrade the membrane and reduce cell longevity. Heat exchangers and thermal insulators are commonly used to maintain uniform temperature distribution across the cell.
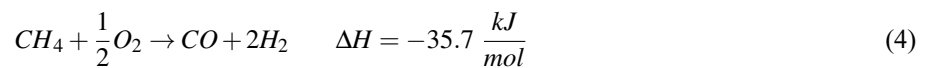
## 2.2 *Autothermal reforming (ATR)*

ATR is a key process in the production of hydrogen and synthesis gas, particularly from hydrocarbons like natural gas. The process integrates exothermic partial oxidation (POX) and endothermic steam reforming (SR) into a single reactor, achieving a thermally balanced system without external heat input. This balance allows for efficient energy utilization, making ATR a favorable approach in industrial applications compared to traditional steam methane reforming (SMR) or POX alone [16].
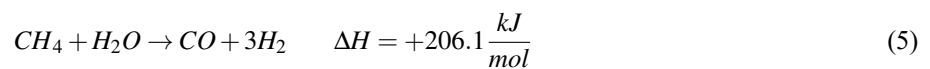
### 2.2.1 *Thermodynamic and kinetic foundations of ATR*
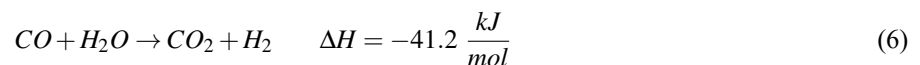
The fundamental reactions involved in ATR include [16, 17]:

1. Partial Oxidation (exothermic):

$$CH_4 + \frac{1}{2}O_2 \rightarrow CO + 2H_2 \qquad \Delta H = -35.7 \frac{kJ}{mol} \tag{4}$$

2. Steam Reforming (endothermic):

$$CH_4 + H_2O \rightarrow CO + 3H_2 \qquad \Delta H = +206.1 \frac{kJ}{mol} \tag{5}$$

3. Water-Gas Shift Reaction (slightly exothermic):

$$CO + H_2O \rightarrow CO_2 + H_2 \qquad \Delta H = -41.2 \frac{kJ}{mol} \tag{6}$$

The total energy balance for the system, combining the heat release from oxidation with the heat demand for steam reforming, provides the autothermal condition. Under this condition, the reactor operates without external heating, as the heat produced by oxidation is consumed by the reforming process. Mathematically, the energy balance for ATR can be represented as:

$$\sum \Delta H_{POX} + \sum \Delta H_{SR} + \sum \Delta H_{WGSR} = 0 \tag{7}$$

This balance ensures optimal performance and minimizes energy losses.

### 2.2.2 *Reactor design and catalytic considerations*

ATR reactors typically consist of two zones: an oxidation zone where partial combustion occurs, followed by a catalytic reforming zone where the remaining methane undergoes reforming. The use of a catalyst, often nickel-based, enhances the steam reforming process. The catalyst must be highly resistant to carbon deposition and thermal sintering due to the high temperatures involved in both the oxidation and reforming reactions [16, 17, 18].

A key design challenge in ATR is maintaining the appropriate oxygen-to-carbon (O/C) ratio, which is critical for avoiding soot formation while ensuring efficient conversion of methane. The typical O/C ratio in ATR processes ranges between 0.5 and 0.6, ensuring a balance between adequate heat generation and the avoidance of excessive carbon formation.

### 2.2.3 *Kinetic modelling*

The kinetics of ATR can be described using Langmuir-Hinshelwood or Eley-Rideal mechanisms, where the surface reactions on the catalyst govern the overall rate of methane conversion. The rate equations for methane reforming typically take the form [16, 17, 18]:

$$r_{SR} = k_{SR} \frac{P_{CH_4} P_{H_2O}}{(1 + K_{CO} P_{CO} + K_{CO_2} P_{CO_2})^2} \tag{8}$$

where $r_{SR}$ is the rate of steam reforming, $k_{SR}$ is the rate constant, and $K_{CO}$ and $K_{CO_2}$ represent the adsorption coefficients for carbon monoxide and carbon dioxide, respectively. Similarly, for the partial oxidation reaction:

$$r_{POX} = k_{POX} \frac{P_{CH_4} P_{O_2}}{(1 + K_{O_2} P_{O_2} + K_{H_2} P_{H_2})} \tag{9}$$

These kinetic models allow for the optimization of reactor conditions by predicting methane conversion rates under different temperatures, pressures, and gas compositions. Advanced computational fluid dynamics (CFD) models are often employed in the design of ATR systems to simulate the complex interplay of heat transfer, chemical reactions, and mass transport in the reactor.

### 2.2.4 *Recent advances and challenges*

Recent research on ATR has focused on improving catalyst stability and performance. Novel catalysts, such as bimetallic and perovskite-based materials, have shown promise in enhancing resistance to carbon deposition and increasing reforming efficiency at lower temperatures. Additionally, the development of ceramic-based reactors and membrane reactors has improved hydrogen yield by selectively removing hydrogen during the reaction process.

However, challenges remain, particularly in scaling ATR systems for larger applications such as hydrogen production for fuel cells or synthetic fuel generation. The high operating temperatures (800–1000 °C) and the need for precise control over reactant flow rates and ratios necessitate advanced control systems. Moreover, improving the carbon capture potential of ATR processes is critical for reducing the overall carbon footprint, especially when used in conjunction with carbon capture and storage (CCS) technologies [16, 17, 18].

## 2.3 *Integrated system*

In the context of the initial assumptions and parameters for modeling the cycle, it is essential to highlight that the values assigned for the system's power generation capacity and the associated components and equipment are based on a reference hybrid system. This reference system, designed as a small-scale electricity generator, possesses a capacity of approximately 1 MW, making it suitable for industrial applications or regions disconnected from the main power grid. The primary components used in this system, such as the PEMFC and the natural gas reforming unit, have been evaluated within the framework of this capacity.

Consequently, the assumptions made for each of these components are aligned with their individual applications, drawing from empirical data provided in the referenced literature. The process of minimizing energy losses across the comprehensive cycle has been a focal point, aiming to enhance the overall efficiency of the system. To achieve this, the development of the proposed cycle and the refinement of the model's accuracy have been conducted through various scenarios discussed in previous sections. Subsequently, strategies for improving efficiency under both standard and non-standard conditions have been proposed.

The proposed CHP system, as illustrated in Figure 1, is composed of several integral components. These include the natural gas preheating system, the gas purification unit, the PEMFC, the heat recovery system with provisions for producing hot water and steam, air preheaters, a water management system, and a steam generation unit essential for the reformer operation.
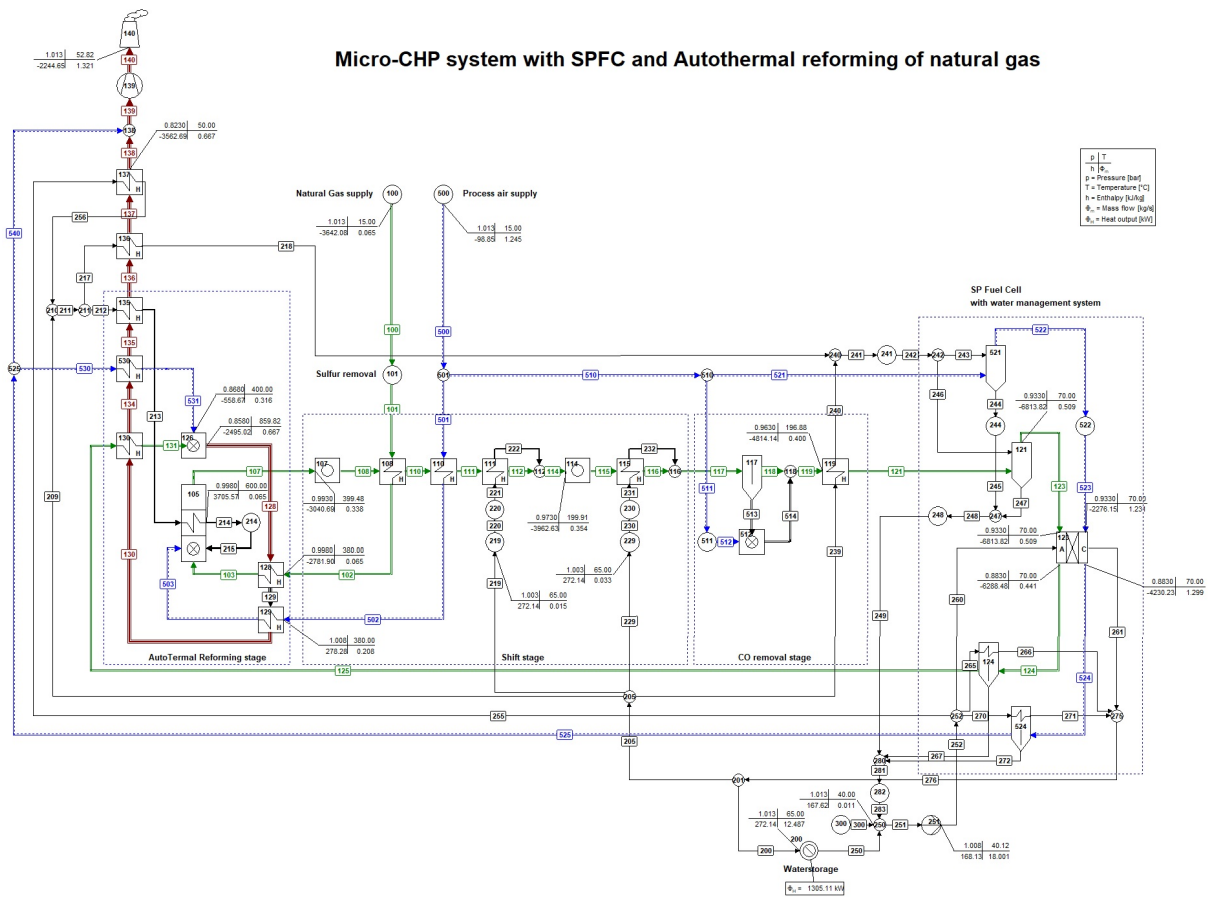


**Figure 1.** Integrated model simulation of the combined heat and power system utilizing a PEMFC and ATR of natural gas

The gases produced from the autothermal reforming process cannot be directly utilized in the fuel cell due to the presence of impurities, which are detrimental to the fuel cell's operation. Therefore, the gas purification system is critical for removing sulfur compounds and carbon monoxide from the reformer's output. This purification process is conducted at a lower temperature to avoid operational and chemical constraints; thus, the gas, initially at a temperature exceeding 480 °C, must be cooled before purification. This cooling occurs through heat exchangers during the shift process, reducing the gas temperature to approximately 130 °C. The heat released in this cooling process is utilized to generate steam, which is then applied within other steam-dependent cycles in the system.

The hot gases exiting the PEMFC, primarily consisting of water vapor and unreacted hydrogen, are processed in a water management system where they are dehumidified. Subsequently, these gases are directed either back to the reformer's combustion chamber or to the system's exhaust stack.

The reformer unit is fundamental in providing the required fuel for the PEMFC, operating on the natural gas reforming mechanism to produce hydrogen-rich fuel. The reformer operates at a temperature of 900 °C and a pressure of 1 bar. The molar composition of the gases produced by the reformer before the shift reaction is detailed in Table 1, while the post-shift reaction gas composition is provided in Table 2.

Table 1. Molar composition of gases from the reformer before shift reaction

| Component | Molar fraction (%) |
|---|---|
| $H_2$ | 36.59 |
| $N_2$ | 31.71 |
| $H_2O$ | 14.77 |
| Ar | 0.35 |
| $CO_2$ | 4.01 |
| CO | 12.56 |

Table 2. Molar composition of gases from the reformer after shift reaction

| Component | Molar fraction (%) |
|---|---|
| $H_2$ | 42.67 |
| $N_2$ | 28.70 |
| $H_2O$ | 14.68 |
| Ar | 0.30 |
| $CO_2$ | 14.10 |
| CO | 0.43 |

The PEMFC, when integrated with the mentioned natural gas reformer, efficiently converts reformed methane into electricity. The hot air expelled from the fuel cell's cathode (off-gas) is recycled to supply the necessary air for the reformer's combustion chamber.

## 2.4 Economic model approach

A comprehensive economic analysis is conducted for the proposed SPFC CHP system with low power generation capacity. Economic indicators such as the internal rate of return (IRR) and net present value (NPV) are calculated based on international fuel and electricity prices. Additionally, the competitiveness of this system is evaluated against conventional power generation methods [19].

The main objectives of the economic model include providing a detailed cost formulation for equipment components and analysing both direct and indirect costs, such as capital costs, operational costs, and general expenses. This analysis fills gaps in previous studies where such parameters were often excluded or only superficially considered. Furthermore, the system's economic feasibility is assessed under current electricity and fuel prices in European and American markets, offering insights into its future competitiveness. The model also estimates key metrics like NPV, IRR, and total system cost, with the results presented in comparative tables and graphs.

### 2.4.1 Total investment costs

Before the operation of a power plant, various expenses must be incurred for the purchase and installation of machinery and equipment. Land and utility services need to be specified and prepared with piping, control systems, and other services. In addition, funds for operating costs must also be secured. The capital required to set up the production facilities is referred to as fixed investment costs, while the funds required for plant operations are called working capital. The total investment cost is the sum of fixed investment and working capital, with major references for this calculation outlined in [20, 21, 22].

Addressing the reviewer's comment on the impact of equipment cost fluctuations, particularly platinum catalyst costs in PEMFCs, on the financial viability of CHP systems across different regions, it's essential to consider how these cost variations influence system economics.

Platinum group metals (PGMs), notably platinum, are integral to PEMFC catalysts. Fluctuations in platinum prices can significantly affect the capital costs of fuel cell systems. For instance, a 10% increase in platinum price can lead to a 5–7% rise in overall system costs, thereby extending payback periods and reducing economic attractiveness [23].

Regional disparities in platinum availability and procurement costs further influence these dynamics. Regions with limited access to platinum resources may face higher procurement costs, adversely impacting the financial feasibility of PEMFC-based CHP systems. Conversely, areas with access to alternative catalysts or localized supply chains can experience shorter payback periods and improved economic feasibility. Incorporating these considerations into the economic model analysis will provide a more comprehensive understanding of how equipment cost fluctuations affect the financial viability of PEMFC-based CHP systems across different regions [24, 25].

To mitigate the impact of platinum price fluctuations, ongoing advancements aim to reduce platinum loadings or utilize platinum-free catalysts, such as nickel or cobalt-based options. These innovations hold promise for improving the economic feasibility of PEMFC-CHP systems over time [26].

### 2.4.2 *Fixed investment costs*

Fixed investment costs for the power plant can be categorized into direct and indirect expenses. Direct costs are associated with equipment procurement, installation, and site preparation, including tools, foundations, and other infrastructure requirements. These direct costs constitute a significant portion of the investment. Indirect costs, although not directly tied to the plant's operation, must be factored in as overhead and include expenses such as engineering supervision and construction. Additionally, unforeseen costs during construction should also be accounted for [27].

### 2.4.3 *Equipment purchase costs*

For calculating equipment purchase costs (EPC), established formulations are used, with adjustments made for economic changes over time using cost indices. Historical data on equipment costs must be updated to reflect current economic conditions using indices such as the Marshall and Swift index, commonly applied for EPC estimations. Moreover, equipment size and capacity also impact costs, as demonstrated by Equation (10). The purchase cost depends not only on size but also on operational parameters such as pressure and temperature, with specific relationships for equipment used in this study's CHP system shown in Table 11 [22].

$$EPC_{S_2} = EPC_{S_1} \left( \frac{S_2}{S_1} \right)^{c_i} \tag{10}$$

In Equation (10), $S_1$ and $S_2$ represent the sizes or scales of the equipment in different scenarios. Specifically, $S_1$ denotes the baseline size of the equipment, while $S_2$ is the target or scaled size. This scaling approach is used to estimate the EPC based on changes in equipment size, where $c_i$ is the scaling exponent that depends on the type of equipment. The value of $c_i$ for each type of equipment is provided in the references [20], with an average value of 0.6 used in the calculations. However, in calculating the cost of equipment, the given equation alone cannot be relied upon, as the price is also influenced by parameters such as operating pressure, temperature, and the material of the equipment. The specific relationships for calculating the main components of the CHP system designed in this study are presented in detail in the sections corresponding to Table 3.

**Cost Function of the Reforming System**

The cost of the natural gas reforming unit has been estimated using Equation (11). The amount of heat absorbed, which is required for the chemical reaction, has been determined in this equation based on the system's energy balance [22].

$$C_{SR} = 0.677 Q^{0.81} \tag{11}$$

In this equation, $C_{SR}$ represents the cost of the steam reformer, and Q denotes the capacity or flow rate of the reformer, typically measured in units relevant to the process (e.g., kg/h or $Nm^3/h$). The coefficient 0.677 and the exponent 0.81 are empirical factors derived from cost estimation data for steam reformers.

**Blower Cost Equations**

The main components of the blower system are like those of a compressor, and its cost formulation is provided by Equation (12). According to these equations, the axial work of the compressor is a key factor influencing the system's costs [28, 29, 30].

$$C_{Comp} = 91526 \left[ \frac{W_{Comp}}{445} \right]^{0.67} \tag{12}$$

In this equation, $C_{Comp}$ represents the cost of the compressor, and $W_{comp}$ denotes the power requirement of the compressor, typically measured in kilowatts. The coefficient 91,526 and the exponent 0.67 are empirical constants obtained from industry data for cost estimation. The denominator, 445, is a reference power value used to standardize the equation.

**Table 3.** Cost equations for SPFC system and other equipment in the CHP system

| Parameter | Cost equation | Equation number |
|---|---|---|
| *SPFC system parameters* | | |
| $P_{SPFC} \times 1500$ | $C_{SPFC}$ | (13) |
| $0.1 \times C_{SPFC}$ | $C_{aux}$ | (14) |
| $10^5 \left( \frac{W_{SPFC}}{500} \right)^{0.7}$ | $C_{inverter}$ | (15) |
| *Other equipment parameters* | | |
| $130 \left( \frac{A_{Heat\ Exchanger}}{0.093} \right)^{0.78}$ | $C_{Heat\ Exchanger}$ | (16) |
| $442 \left( W_{Pump}^{0.71} \right) \times 1.41 f_n$ | $C_{Pump}$ | (17) |
| $N \times 4000$ | $C_{Saturator}$ | (18) |
| $N \times 3500$ | $C_{Reactor}$ | (19) |

where,

$P_{SPFCP}$: Power output of the SPFC, typically measured in kW.

$C_{SPFC}$: Cost of the SPFC unit.

$C_{aux}$: Auxiliary equipment cost associated with the SPFC system, calculated as a percentage of $C_{SPFC}$.

$W_{SPFC}$: Electrical power capacity of the inverter for the SPFC, typically measured in watts.

$C_{inverter}$: Cost of the inverter associated with the SPFC system.

$A_{Heat\ Exchanger}$: Surface area of the heat exchanger, used in calculating the heat exchanger cost.

$C_{Heat\ Exchanger}$: Cost of the heat exchanger, determined based on its surface area.

$W_{Pump}$: Power requirement of the pump, typically measured in kW.

$C_{Pump}$: Cost of the pump, calculated based on its power requirement and additional factors.

$f_n$: Efficiency correction factor for the pump.

N: Quantity or number of units, used in determining the costs of certain equipment components, such as the saturator and reactor.

$C_{Saturator}$: Cost of the saturator, calculated based on the quantity N.

$C_{Reactor}$: Cost of the reactor, also based on the quantity N.

**Gas Purification System Cost Equations**

Equations (20) and (21) are used to calculate the costs associated with the gas purification system. For desulfurization and particle separation from the syngas produced in the reforming system, a combination of a cyclonic separator with a ceramic membrane and filter can be utilized [22].

$$C_{Sep} = 35A_{mem} \qquad (20)$$

$$C_{Filter} = 3800A_{Filter}^{0.52} \qquad (21)$$

**Cost Equations for Other CHP System Components**

The cost of other major equipment used in the CHP system, not previously mentioned in the subsystems, is estimated using Equations (16) to (19), as shown in Table 3. These components include:

- Heat exchangers used as air and fuel preheaters in the cycle [31].

- Pumps are used to increase the pressure of water or steam streams in the system [21, 22]. In the cost function for pumps, the efficiency correction factor is calculated using Equation (22), as provided below:

$$f_\eta = 1 + \left( \frac{1 - 0.8}{1 - \eta_{Pump}} \right) \qquad (22)$$

- A chimney, which in this study is used for the exhaust of gases from the steam generator needed by the reformer.

### 2.4.4 *Assumptions*

Several key assumptions have been made for solving the presented economic model, which are outlined as follows:

- The financial analysis of the proposed CHP system power plant is based on banking standards. The equity ratio is 70:30 of the total investment, with 70% being a bank loan and 30% private sector investment. The interest rate for loan repayment is assumed to be 12%.

- The overall system lifespan is assumed to be 25 years. However, we acknowledge that certain components, particularly those in the fuel cell system, such as the membrane and catalysts, may require replacement during this period due to degradation over time. The costs associated with periodic replacement of these components have been factored into the maintenance and operational expenses to reflect a more realistic financial analysis.

- Based on available data for the guaranteed purchase price of electricity from renewable sources in industrial units in Iran, the electricity price is assumed to be US$ 0.1/kWh. Additionally, due to the significant price difference for electricity sales between European countries and the United States, two benchmarks have been considered for electricity prices. The average electricity price for industrial sectors is US$ 0.16/kWh in Europe and US$ 0.08/kWh in the United States [32, 33].

- The price of natural gas for industrial use in Iran is set at US$ $0.1/m^3$. The prices of natural gas for industrial use in Europe and the United States are US$ $0.4/m^3$ and US$ $0.073/m^3$, respectively, in the calculations [32, 33].

# 3. System modeling

## 3.1 *Modeling constraints*

When modeling the system, both technical and structural constraints must be considered. The structural constraints largely stem from the inherent nature of the process, specifically the characteristics of the CHP cycle. Regarding technical constraints, these can be categorized into two main groups:

- Application Constraints: These include factors such as the availability of fuel, the necessity of purifying the syngas produced by the reformer unit, and other related considerations.

- Operational Constraints: Examples include the need to humidify the air and fuel before they enter the fuel cell, the requirement to use a moisture separator at the fuel cell's exhaust, and concerns related to the dew point of exhaust gases from the cycle.

## 3.2 *Model implementation*

The model implementation involves establishing connections between the various components of the proposed CHP system, defining environmental conditions, inputting initial values, and making assumptions for each section. Once the model is executed, the modeling process is completed. The primary objectives of this model implementation are:

- To generate both heat and power within a comprehensive cycle.

- To reduce heat losses by creating logical connections between heat-consuming and heat-generating units, and by determining the conditions that affect them.

- To produce the necessary gaseous fuel for direct power generation (via the fuel cell) within the cycle.

## 3.3 *Preliminary considerations*

1. To achieve higher efficiency in the SPFC-based CHP system, the following design considerations were made:

- Utilization of combustible gases from the reformer system's combustion chamber directly within the cycle.

- Exploitation of the heat released when cooling the gases exiting the autothermal reforming unit before the gas purification unit, to supply the steam required for the reformer.

- Use of part of the heat from the gases exiting the natural gas reformer to preheat the incoming fuel and air.

- Implementation of humidified air in the cathode of the SPFC by utilizing a humidifier unit.

- Use of water separation units to manage the water used in the system and to recycle it for humidifying the incoming fuel and air to the fuel cell.

2. Considering the use of an SPFC system with a constant power output of 1 MW to achieve the desired power output, the operational and output pressures in the natural gas reforming process were set at 1 bar.

3. Heat generation in the combustion chamber of the reforming system, along with the utilization of heat recovery units within the studied CHP cycle, has created the capacity to produce hot water for use in auxiliary units.

## 3.4 *Initial model assumptions*

To analyze the system and achieve mass and energy balance for the cycle, the Cycle-Tempo software was employed to create a model under steady-state conditions [34]. Therefore, a model comprising subsystems such as the autothermal natural gas reforming system, the gas purification system including an evaporator, the PEMFC, and a heat recovery system consisting of a network of heat exchangers producing steam or hot water, was developed. Achieving convergence in the calculations of these subsystems was the primary goal throughout the modeling process. Some of the assumptions used in creating the model are as follows:

- The system operates under steady-state conditions.

- The system's operation is considered adiabatic.

- Issues arising from the formation of pollutants, residues, alkali metals, etc., are disregarded.

- In the water supply section of the CHP system, an isentropic efficiency of 80% is assumed for the pump.

- The isentropic efficiency of the blower or compressor is 80%.

- The mechanical efficiency of the blower or compressor is assumed to be 100%.

- Pressure drops in the heat exchangers are considered minimal.

The temperature and pressure of the system's inputs are shown in Table 4.

**Table 4.** Temperature and pressure of fuel, air, and water inputs to the system

| Source | Temperature (°C) | Pressure (bar) |
|---|---|---|
| Natural Gas | 15 | 1.013 |
| Air | 15 | 1.013 |
| Water* | 65 | 1.013 |

\* Water input to the steam supply system for the reformer

The operating temperature of the fuel cell is 70 °C, and the operating pressure is 1 bar. The fuel cell's surface area is 700 m$^2$, and the fuel utilization factor in the fuel cell is 0.8. The efficiency of the fuel cell's DC/AC converter is also assumed to be 96%.

## 3.5 *Quantitative approach*

Table 5 summarizes the quantitative approach for the PEMFC/ATR system, detailing the critical parameters such as capacity, natural gas flow rate, and conditions at both the inlet and outlet of the system.

**Table 5.** Quantitative approach for PEMFC/ATR system

| Parameter | Value |
|---|---|
| Combined heat and power capacity | 2487.61 kW |
| Mass flow rate of natural gas | 0.06546 kg/s |
| Inlet temperature of natural gas | 15 °C |
| Inlet pressure of natural gas | 1 bar |
| Outlet pressure from ATR reformer | 0.993 bar |
| Outlet temperature from ATR reformer | 600 °C |

1. Saturated Steam and Reformer Operations: Saturated steam at 105 °C is introduced into the reformer, where it is heated to 600 °C to facilitate the reforming reactions. Natural gas enters the reformer at 440 °C with a mass flow rate

of 0.065 kg/s, and after the reactions occur, the produced gas exits the reformer at 400 °C before entering the reactor. The inlet air, with a temperature of 45 °C and a mass flow rate of 4.336 kg/s, is directed towards the reformer. This air is preheated to 400 °C using a heat exchanger before being mixed with the incoming fuel and air. Hot gas at approximately 860 °C with a mass flow rate of 0.667 kg/s provides the necessary heat for the reforming reactions. The heat from this hot gas is also utilized for preheating the air and generating the saturated steam required by the system.

2. Shift Process Operations: During the shift process, the produced gas is first heated to 265 °C. Subsequently, steam is introduced in two stages, with mass flow rates of 0.015 kg/s and 0.387 kg/s, respectively, to react with the gas. Finally, the gas exits the system at approximately 130 °C.

3. Carbon Monoxide Removal Unit: In the carbon monoxide separator unit, the toxic CO content is absorbed from the produced gas. The outgoing gas is then cooled to 130 °C using a heat exchanger.

4. Humidification of Fuel and Air: The fuel and air, with mass flow rates of 0.4 kg/s and 1.025 kg/s, respectively, are introduced into humidification units before entering the PEMFC. Water at 75 °C is introduced into both humidification systems and exits at 40 °C. The humidified fuel and air, with temperatures of 70 °C and mass flow rates of 0.509 kg/s and 1.231 kg/s, respectively, exit the humidification units before being directed to the anode and cathode of the fuel cell.

5. Fuel Cell Operations: The fuel cell operates at 70 °C and generates 1000 kW of electrical power. As previously noted, not all the input fuel to the SPFC stack is converted to power; the fuel utilization factor is 80%.

6. Exhaust Gas Management: The exhaust gases from the fuel cell's anode, which contain some unreacted hydrogen, have a mass flow rate of 0.441 kg/s and a temperature of 70 °C. These gases are directed to a water separation unit for dehumidification. Similarly, the air exiting the fuel cell's cathode, with a temperature of 70 °C and a mass flow rate of 1.229 kg/s, also enters the water separation unit. In the dehumidification units, 0.089 kg/s and 0.239 kg/s of water are extracted from the fuel and air streams, respectively. These streams are then directed towards the natural gas reforming process to aid in heat generation.

7. Electrical Efficiency: The electrical efficiency of the combined heat and power system in this study is calculated to be 40.2%. The energy absorbed by the system through the input fuel is 2487.61 kW, with the system producing approximately 1000 kW of electricity. However, due to the consumption of some of the generated electricity by the system's pump and compressor, the net efficiency is determined to be 38.67%.

8. Thermal Efficiency: As previously mentioned, the potential for absorbing 1305.11 kW of thermal energy through the production of hot water in the proposed CHP system's water management unit results in a thermal efficiency of 52.46%. Therefore, the overall CHP system efficiency, which combines net electrical and thermal efficiencies, is calculated to be 91.13%.

In Table 6, the input energy to the system via natural gas and the electricity produced by the fuel cell is detailed.

**Table 6.** Comparison of input energy and output electricity from the system

| Component | Natural gas (kW) | Pump (kW) | Compressor (kW) | PEMFC output (kW) |
|---|---|---|---|---|
| Absorbed power | 2487.61 | 0.51 | 37.48 | - |
| Output power | - | - | - | 1000 |

## 3.6 Process description

Natural gas and air are introduced into the system, where a portion of the incoming air reacts with the natural gas, while the remaining air is directed to the fuel cell. After passing through heat exchangers and experiencing a temperature

increase, the natural gas and air enter the reformer. Within the reformer, the reactions, as detailed in the previous chapter, occur at a temperature of 900 °C. The reaction products exit the reformer at a temperature of 600 °C. The byproduct gases generated during the process pass through heat exchangers, where their temperature is reduced, and the absorbed heat is reintroduced into the system.

The reformer's output is directed into a reactor where; after passing through several heat exchangers, sulfur is removed from the gas. Additionally, CO, a toxic gas, is eliminated as the gas mixture enters a separation unit. Ultimately, the produced gaseous fuel is supplied to the fuel cell for electricity generation. In the fuel cell, the air, after being saturated in a humidifier unit, is combined with the reaction product, which also undergoes saturation in another humidifier unit before entering the fuel cell. After exiting the fuel cell and passing through a moisture separator, the water generated during the process is stored in a water storage tank, while the remaining gases are expelled through a chimney after undergoing heat recovery.

Table 7 presents the assumptions related to the combined heat and power cycle under study. The pressure drops considered for modeling the heat exchanger network in the proposed combined heat and power system are shown in Table 8.

**Table 7.** Process-related assumptions

| Parameters | Values (unit) |
|---|---|
| Mechanical efficiency (compressor) | 100% |
| Isentropic efficiency (compressor) | 80% |
| Autothermal reforming system | |
| Steam temperature | 600 °C |
| Steam pressure | 1 bar |
| Air temperature | 400 °C |
| Natural gas flow rate | 0.065 kg/s |
| Combustion chamber pressure (reformer) | 1 bar |
| Temperature | 900 °C |

**Table 8.** Pressure drops in heat exchangers used in the system

| Heat exchanger (No.) | Pressure drop (bar) |
|---|---|
| $\Delta P_{137, \text{both sides}}$ | 0.004 |
| $\Delta P_{136, \text{both sides}}$ | 0.004 |
| $\Delta P_{135, \text{both sides}}$ | 0.005 |
| $\Delta P_{530, \text{both sides}}$ | 0.002 |
| $\Delta P_{130, \text{both sides}}$ | 0.005 |
| $\Delta P_{129, \text{both sides}}$ | 0.005 |
| $\Delta P_{128, \text{both sides}}$ | 0.005 |
| $\Delta P_{108, \text{both sides}}$ | 0.005 |
| $\Delta P_{110, \text{both sides}}$ | 0.004 |
| $\Delta P_{111, \text{both sides}}$ | - |
| $\Delta P_{115, \text{both sides}}$ | - |
| $\Delta P_{119, \text{liquid side}}$ | 0.005 |
| $\Delta P_{119, \text{gas side}}$ | 0.01 |

Figures 1–5 depict the main units modeled within the CHP system studied in this research.
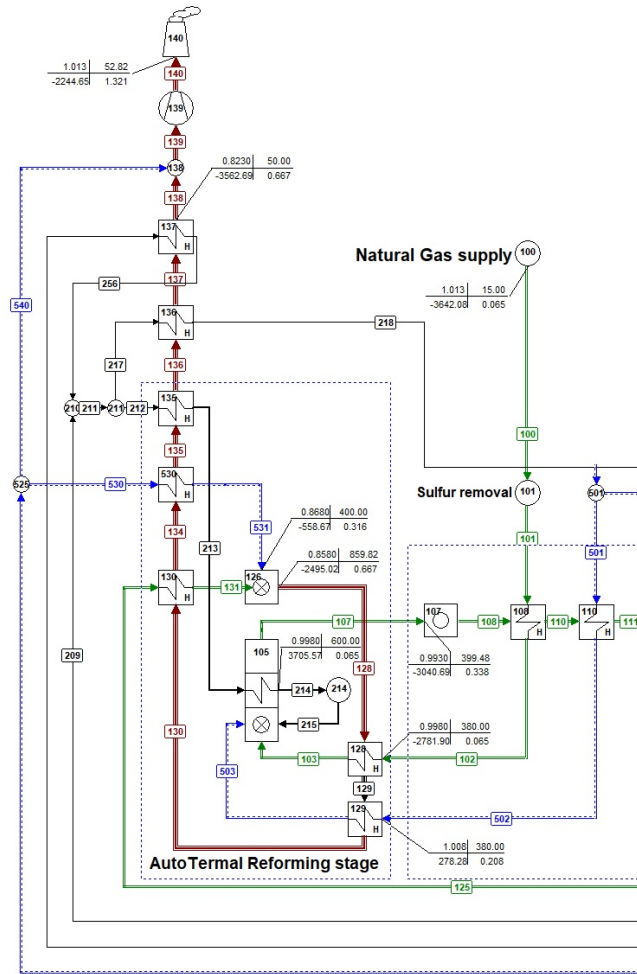
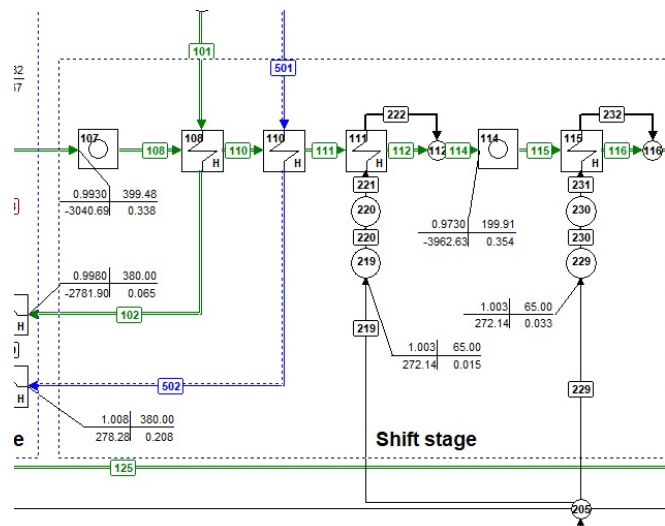**Figure 2.** Simulated model of the ATR system for natural gas



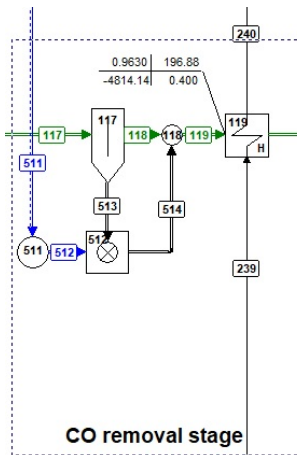**Figure 3.** Simulated model of the shift process

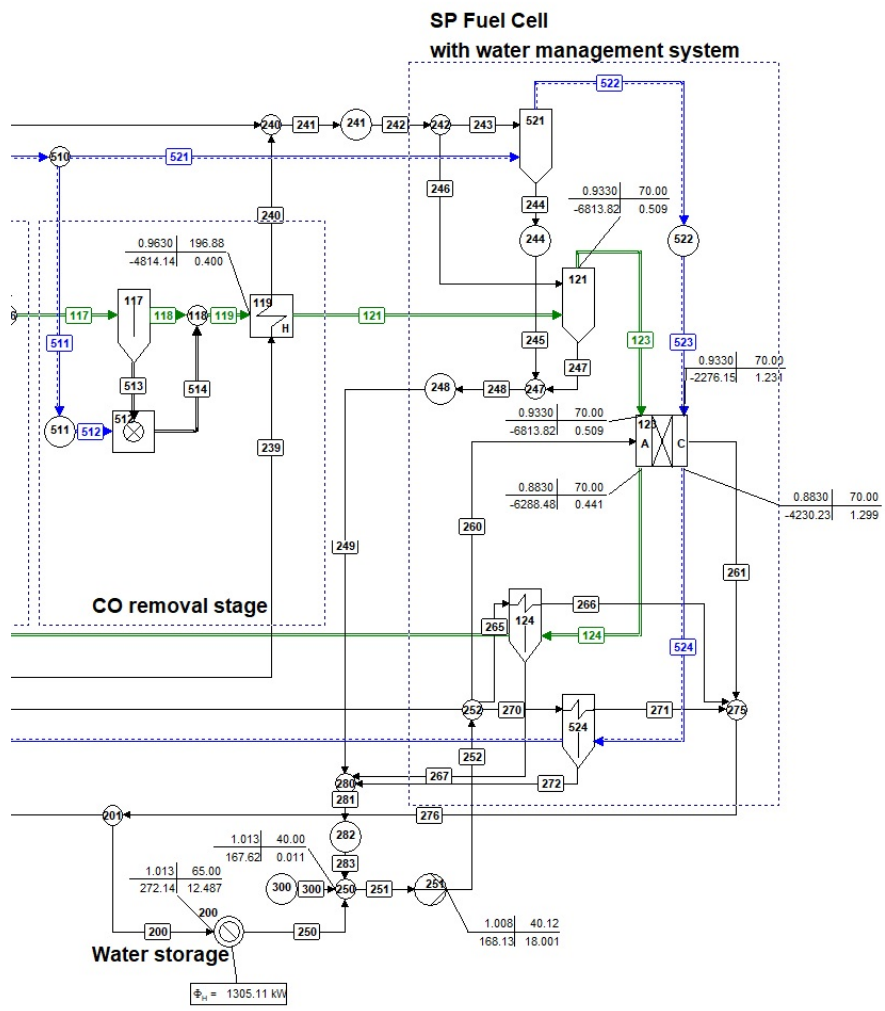**Figure 4.** Simulated model of the carbon monoxide removal process



**Figure 5.** Simulated model of the PEMFC with water management

# 4. Results and discussions

The results of the key output parameters for the CHP system analyzed in this study are presented in Table 9.

**Table 9.** Results of the main parameters for the CHP system under study

| Parameter (Unit) | Value |
|---|---|
| Natural gas consumption (kg/hr) | 224 |
| Electrical power output of SPFC (kW) | 1000 |
| Inlet temperature to fuel cell (°C) | 70 |
| Outlet temperature from fuel cell (°C) | 70 |
| Fuel cell reaction temperature (°C) | 700 |
| Pressure drop at fuel cell inlet (bar) | 0.05 |
| Pressure drop at fuel cell outlet (bar) | 0.05 |
| Water mass flow rate at SPFC inlet (kg/s) | 0.99 |
| Water mass flow rate at SPFC outlet (kg/s) | 1.221 |
| SPFC cell voltage (V) | 0.7236 |
| Power density in SPFC (kW/m$^2$) | 1.93 |
| PSOFC current density (A/m$^2$) | 4000 |
| Required fuel cell area (m$^2$) | 2500.44 |
| Exhaust gas flow rate from the stack (ton/day) | 114.13 |
| Exhaust gas temperature from the stack (°C) | 52.82 |
| Net electrical efficiency of the system (%) | 38.1 |
| Net thermal efficiency of the system (%) | 46.1 |
| Overall CHP efficiency of the system (%) | 91.3 |

## 4.1 *Parametric analysis*

To examine the effect of each variable on efficiency (temperature, pressure, and humidity), we analyze the trend of efficiency changes by holding two variables constant and varying the third.

The process efficiency was studied at temperatures of 15, 20, 25, 30, 35, and 40 degrees Celsius, while keeping other variables constant (pressure at 1 bar and humidity at 60%). The efficiency results for the CHP system are provided in Table 10.

**Table 10.** Changes in overall system efficiency of CHP with variations in ambient temperature

| Temperature (°C) | Heat absorbed by system (kW) | Thermal efficiency (%) | Net electrical efficiency (%) | Overall efficiency (%) |
|---|---|---|---|---|
| 15 | 1305.11 | 52.44 | 38.23 | 91.22 |
| 20 | 1271.10 | 52.41 | 38.68 | 91.08 |
| 25 | 1235.56 | 52.38 | 38.89 | 91.40 |
| 30 | 1204.44 | 52.35 | 38.90 | 91.25 |
| 35 | 1178.34 | 52.31 | 38.95 | 91.24 |
| 40 | 1137.96 | 52.29 | 38.70 | 91.00 |

As observed, changes in ambient temperature result in an increase in the overall efficiency of the CHP system under study. This is due to the increased hydrogen production capacity in the reforming system, as the load on the heat exchangers decreases with higher ambient temperatures. Consequently, more power can be produced with the same fuel input. However, as shown in Table 11, this increase is primarily attributed to the rise in thermal efficiency of the CHP system, with most of the changes resulting from the improved performance of the heat exchanger network.

**Table 11.** Changes in overall system efficiency of CHP with respect to variations in ambient humidity

| Ambient humidity (%) | Heat absorbed by system (kW) | Thermal efficiency (%) | Net electrical efficiency (%) | Overall efficiency (%) |
|---|---|---|---|---|
| 40 | 1299.93 | 52.30 | 38.52 | 90.88 |
| 50 | 1307.51 | 52.44 | 38.66 | 91.00 |
| 60 | 1305.11 | 52.44 | 38.73 | 91.32 |
| 70 | 1307.44 | 52.57 | 38.86 | 91.58 |
| 80 | 1309.95 | 52.90 | 38.94 | 91.86 |
| 90 | 1311.21 | 52.99 | 38.99 | 92.08 |

In another study, at a temperature of 15 °C and a pressure of 1 bar, the ambient humidity varied from 40% to 90%. The efficiency resulting from these humidity changes is presented in Table 11.

As demonstrated, variations in ambient humidity contribute to enhancing the overall efficiency of the CHP system under investigation. This improvement can be attributed to the increased moisture content in the air supplied to the hydrogen production unit within the reforming system. With higher humidity, the system's capacity to produce syngas is augmented due to the additional water content available for the reformer process. As illustrated in Table 11, the rise in ambient humidity enhances the water content in both the reforming and water-gas shift processes, resulting in a notable increase in the system's combined heat and power efficiency.

From a thermodynamic standpoint, maintaining a stable ambient temperature while increasing humidity in the intake air has favorable implications for the mass and energy balances of the system. However, it is critical to recognize the operational challenges associated with elevated humidity levels. These include potential issues such as cavitation and corrosion, which could impose significant constraints on system performance. Such conditions may compromise the standard operational environment, thereby leading to increased maintenance costs and operational risks. Therefore, while humidity adjustment offers efficiency benefits, it also introduces complexities that must be carefully managed to avoid detrimental impacts on system integrity and cost efficiency.

While our parametric analysis provides valuable insights into the temperature and humidity dependencies of PEMFC performance, we recognize the importance of experimental validation to support these findings. Studies by Chugh et al. [35] and Subin et al. [36] offer experimental evidence showing how PEMFC performance varies under different environmental conditions. For example, these studies highlight that PEMFC efficiency can decrease by approximately 5–10% under lower humidity levels or higher temperatures due to membrane dehydration effects, which limits proton conductivity. The consistency between our model predictions and these empirical findings reinforces the validity of our theoretical framework. Future work should incorporate experimental testing under a range of temperature and humidity levels to further substantiate these trends and refine the model's accuracy for real-world applications.

## 4.2 *Economic analysis results and discussion*

A parametric analysis was conducted to evaluate the changes in NPV and IRR based on varying electricity prices across different geographic regions. The price range considered spans from US$/kWh 0.1, which corresponds to the electricity sale price in Iran, to US$/kWh 0.2, representing the maximum price in the European Union. As illustrated in Figure 6, the variations in NPV calculated over the operational period of the cycle are presented. It is essential to note that negative NPV values indicate the cycle is not economically viable under those conditions and, therefore, such results are excluded from the acceptable outcomes of the model.

Moreover, the IRR is determined at the point where the NPV equals zero, considering the discount rates applied. These results are shown in Figure 6. As observed, the current cycle yields the highest positive NPV with the electricity prices considered for Europe, while the lowest positive values are seen for Iran and the United States. Two critical points should be considered here: first, electricity prices in several countries around the world already exceed US$/kWh 0.2; and second, the inevitable rise in energy consumption and electricity prices in the coming years. Therefore, the proposed cycle presents a solid economic potential in future energy supply scenarios, making it a suitable option for industries with electricity consumption profiles that align with the proposed cogeneration system.

As highlighted, the system exhibits a better economic outlook in Europe compared to Iran and the United States, as evidenced by the results in Figures 6 and 7. This is primarily due to higher electricity prices in Europe. Furthermore, given the lower fuel costs in Iran, an increase in the feed-in tariff for renewable electricity or the full implementation of subsidy reforms would result in significant growth in NPV and IRR compared to the other two case studies. On the other hand, a mere increase of US¢/kWh 20 in the electricity price in the United States would result in a substantial positive NPV for the proposed system.

Additionally, Table 12 provides the system's payback period for various electricity price points across the case studies previously discussed.
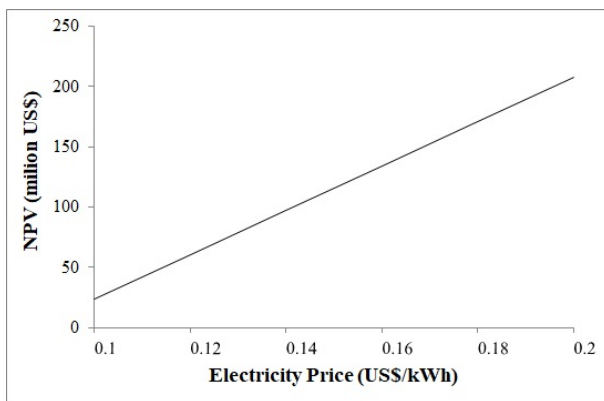


**Figure 6.** NPV variations for the case studies based on different electricity purchase prices
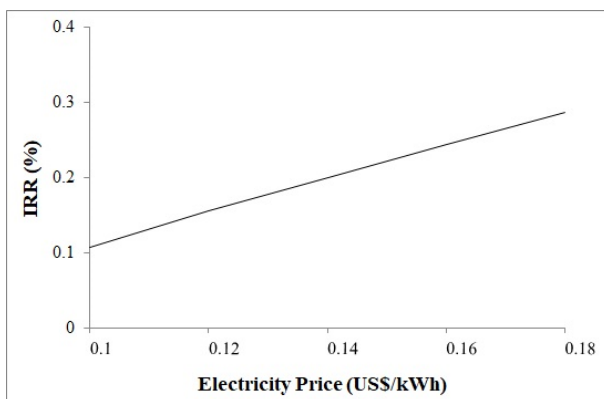


**Figure 7.** IRR variations for the case studies based on different electricity purchase prices

**Table 12.** Break-even point (B.E.P.) of the payback period for the case studies

| Electricity price (US$/kWh) | B.E.P. (years) |
|---|---|
| 0.1 (Electricity price in Iran) | 8.3 |
| 0.12 | 6.2 |
| 0.14 | 4.9 |
| 0.16 (Electricity price in Europe) | 4.0 |
| 0.18 | 3.5 |
| 0.20 | 3.1 |

In Table 13, the estimated EPC costs for various components of the cogeneration system, as previously discussed, are presented. As indicated in Table 13 and Figure 8, the purchase cost of the SPFC for electricity generation is significantly

higher compared to other sections of the power plant. The primary reason for this is the expensive materials used in the fuel cell stack.

**Table 13.** Equipment purchase costs for the proposed cogeneration system

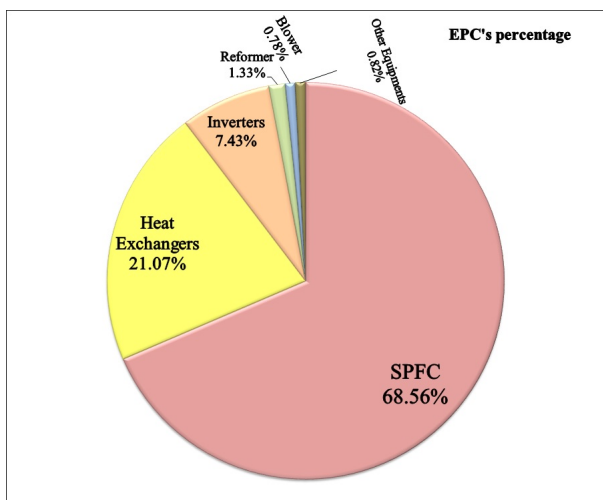| Equipment | Cost (US$) |
|---|---|
| Solid Polymer Fuel Cell (SPFC) | 1,500,000 |
| Heat exchangers | 460,929 |
| Inverters | 162,450.5 |
| Natural gas reformer | 29,193.22 |
| Blowers | 17,142.53 |
| Other equipment | 17,995.49 |
| Total equipment purchase cost | 2,187,710.69 |



**Figure 8.** Distribution of equipment purchase costs for the proposed cogeneration system

Several efforts have been made by manufacturers to reduce the production costs of polymer fuel cell systems, with the goal of cutting the current costs by more than half. Recent advancements in polymer electrolyte membranes have further enhanced the efficiency and durability of SPFCs, focusing on improving proton conductivity and operational stability. For example, composite membranes incorporating nanoscale materials, such as alumina ($Al_2O_3$), have demonstrated significant improvements in ionic conductivity and structural integrity under varied temperature conditions. Studies, such as those by Mohamed et al. [37], emphasize the role of $Al_2O_3$ nanoparticles in enhancing ion transport properties by modifying membrane nanostructure, making these membranes suitable for high temperature applications [38]. Additional advancements include novel materials and electrode fabrication techniques that significantly enhance fuel cell durability, as highlighted by Grandi et al. [39]. Furthermore, recent research has focused on medium-temperature fuel cell applications, using innovative polymer electrolyte membranes like cross-linked polyimide and hydrophobic protic ionic liquids, which enhance fuel cell durability and performance under medium-temperature conditions [40].

Among the estimated costs for other equipment in the cycle, the heat exchangers and DC/AC converters rank next as the most expensive components. New inverter technologies have also been targeted by manufacturers to achieve cost reductions in production [41].

### 4.3 *Environmental assessment of the proposed cycle*

While the use of renewable energy sources, particularly fuel cells, often results in a significant reduction of solid and gaseous emissions in power generation systems, the emission of gaseous pollutants is unavoidable in cogeneration systems based on fuel cells. Furthermore, the environmental assessment of the proposed hybrid system becomes even more critical

due to the use of natural gas and its reforming process. This is because the reforming of natural gas leads to the production of gaseous pollutants from the combustion process in the form of carbon compounds.

Considering the above considerations, this study focuses on methods to improve the overall efficiency of the hybrid system based on SPFCs and to calculate the emissions resulting from the system's operation. A key distinguishing factor of this study compared to previous research is the integrated approach to both efficiency improvement and environmental analysis for such systems.

Table 14 presents the composition of exhaust gases from the chimney of the CHP system proposed in this research, compared to the exhaust gases from a conventional gas turbine system. Additionally, a representation of the gas turbine system model under study is shown in Figure 9.
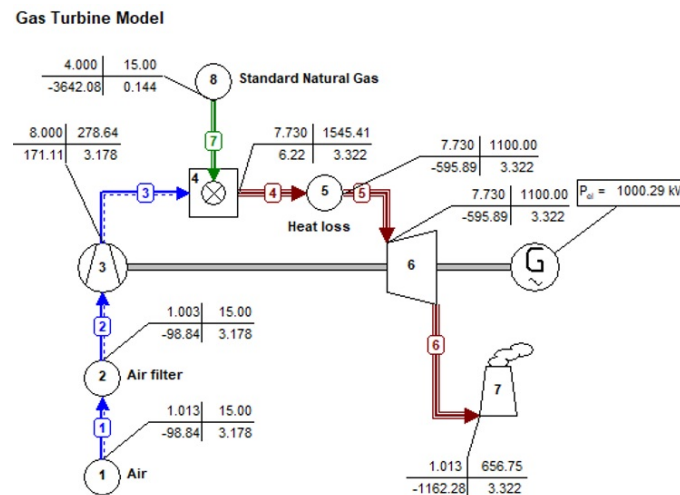


**Figure 9.** A modelled gas turbine system for comparing fuel consumption and emissions production

**Table 14.** Comparison of the molar fractions of exhaust gases between the proposed cogeneration system and a conventional gas turbine

| Compound name | Proposed cogeneration system (molar fraction) | Gas turbine system (molar fraction) |
|---|---|---|
| Carbon Dioxide ($CO_2$) | 6.72% | 5.47% |
| Oxygen ($O_2$) | 5.38% | 8.83% |
| Nitrogen ($N_2$) | 71.51% | 73.38% |
| Argon (Ar) | 0.84% | 0.86% |
| Water ($H_2O$) | 15.10% | 11.45% |

It is worth noting that the electrical power output for both systems being compared is identical at 1000 kW. Additionally, the fuel used in the gas turbine system is natural gas, with the same specifications as the natural gas used in the proposed cogeneration system. This consistency also applies to the characteristics of the air entering both systems.

A key point of comparison between the environmental impacts of the proposed cogeneration system and a conventional gas turbine system lies in the natural gas consumption and the exhaust gases emitted by both systems, which have the same power capacity. This comparison is presented in Table 15.

**Table 15.** Comparison of input and output parameters between the proposed cogeneration system and a conventional gas turbine system

| Component name | Proposed cogeneration system | Gas turbine system |
|---|---|---|
| Natural gas flow rate (kg/s) | 0.065 | 0.144 |
| Exhaust flow rate (kg/s) | 1.321 | 3.322 |
| Annual $CO_2$ emissions (tons) | 2799 | 6191 |

As shown in Table 15, the proposed cogeneration system exhibits a significantly lower consumption of natural gas and a reduction in carbon dioxide emissions compared to a gas turbine system with the same capacity.

Considering the objectives set for sustainable energy development and greenhouse gas reduction, these findings highlight one of the key environmental advantages of implementing the proposed system in this study.

## 5. Conclusions

This study offers an in-depth analysis of the technical, economic, and environmental performance of a large-scale PEMFC-CHP system integrated with ATR of natural gas, addressing key gaps in current research on the scalability and industrial applicability of such systems. The results highlight several critical findings across various dimensions:

- The system demonstrated an impressive overall efficiency of 91.3%, with electrical efficiency reaching 38.1% and thermal efficiency at 46.1%. By optimizing operating conditions such as temperature and humidity, the system's performance was further enhanced, with maximum efficiency reaching 92.08% under high-humidity conditions. The efficient heat recovery and integration of ATR with PEMFC allowed the system to utilize available resources effectively, converting more energy into usable forms compared to conventional systems. This highlights the system's potential to significantly improve the energy output of industrial-scale applications, particularly in sectors requiring both heat and power.

- The parametric analysis revealed that the economic performance of the system is highly dependent on regional electricity prices, making it more viable in areas with higher energy costs. Europe emerged as the most favorable region, with a payback period of just 4.0 years at an electricity price of US$/kWh 0.16, accompanied by the highest NPV. In contrast, Iran's lower electricity prices extended the payback period to 8.3 years. The study also demonstrated the system's adaptability to fluctuating market conditions, particularly in the U.S., where a 20% increase in electricity prices substantially improved the NPV and reduced the payback period. These results underscore the flexibility of the system to respond to varying market dynamics, making it a promising solution for regions with diverse economic conditions.

- From an environmental perspective, the PEMFC-CHP system exhibited substantial reductions in greenhouse gas emissions, achieving a 50% reduction in $CO_2$ emissions compared to conventional gas turbine systems with the same power output. This is particularly important in the context of global efforts to mitigate climate change and adhere to increasingly stringent environmental regulations. The system's lower natural gas consumption (0.065 kg/s) compared to gas turbines (0.144 kg/s) further emphasizes its environmental benefits, making it a highly efficient option for industries looking to reduce their carbon footprint while maintaining operational efficiency.

- The study provides valuable insights into the practical scalability of PEMFC-CHP systems for industrial use, highlighting how advanced integration of ATR technology can overcome many of the limitations faced by traditional power systems. The modular nature of the system allows it to be scaled according to specific energy demands, making it suitable for a wide range of industrial applications. The successful demonstration of both high efficiency and economic viability in larger-scale scenarios is a significant step forward in promoting the adoption of PEMFC-CHP systems across industries, particularly in sectors where energy efficiency and sustainability are paramount.

## Conflict of interest

There is no conflict of interest for this study.

# References

[1]  Z. Zhou, P. Liu, and Z. Li, "Combined heat and power systems: Economic and environmental impact analysis," *Energy Environ. Sci.*, vol. 15, no. 8, pp. 567–590, 2022. https://doi.org/10.1039/C2EE21645A.

[2]  H. A. Ozgoli, S. Safari, and M. H. Sharifi, "Integration of a biomass-fueled Proton Exchange Membrane Fuel Cell system and a Vanadium Redox Battery as a power generation and storage system," *Sustain. Energy Technol. Assess.*, vol. 42, p. 100896, 2020. https://doi.org/10.1016/j.seta.2020.100896.

[3]  Z. Shang, M. M. Hossain, R. Wycisk, and P. N. Pintauro, "Poly(phenylene sulfonic acid)-expanded polytetrafluoroethylene composite membrane for low relative humidity operation in hydrogen fuel cells," *J. Power Sources*, vol. 532, p. 231375, 2022. https://doi.org/10.1016/j.jpowsour.2022.231375.

[4]  N. P. Bayendang, M. T. Kahn, and V. Balyan, "Combined cold, heat and power (CCHP) systems and fuel cells for CCHP applications: a topological review," *Clean Energy*, vol. 7, no. 2, pp. 436–491, 2023. https://doi.org/10.1093/ce/zkac079.

[5]  R. Escobar-Yonoff, D. Maestre-Cambronel, S. Charry, A. Rincón-Montenegro, and I. Portnoy, "Performance assessment and economic perspectives of integrated PEM fuel cell and PEM electrolyzer for electric power generation," *Heliyon*, vol. 7, no. 3, p. e06506, Mar. 2021. https://doi.org/10.1016/j.heliyon.2021.e06506.

[6]  S. Montazerinejad, Y. Zhu, and E. Roberts, "Combined heat and power using high-temperature proton exchange membrane fuel cells: Efficiency and environmental benefits," *Int. J. Hydrog. Energy*, vol. 48, no. 10, pp. 1523–1535, 2023. https://doi.org/10.1016/j.ijhydene.2023.01.067.

[7]  G. Loreti, A. L. Facci, and S. Ubertini, "High-efficiency combined heat and power through a high-temperature polymer electrolyte membrane fuel cell and gas turbine hybrid system," *Sustainability*, vol. 15, no. 22, p. 12515, 2023. https://doi.org/10.3390/su132212515.

[8]  R. Sivaraman, R. Shankar, and K. Venkatesan, "Autothermal reforming of natural gas for hydrogen production: A review," *J. Clean Prod.*, vol. 172, pp. 2631–2646, 2023. https://doi.org/10.1016/j.jclepro.2023.11.188.

[9]  M. Wei, T. Lipman, A. Mayyas, S. H. Chan, D. Gosselin, H. Breunig, et al., *A Total Cost of Ownership Model for High-Temperature PEM Fuel Cells in CHP Applications*. Berkeley, CA, USA: Lawrence Berkeley National Laboratory, 2023. https://doi.org/10.2172/1487582.

[10] I. Pilatowsky, R. J. Romero, C. A. Isaza, S. A. Gamboa, W. Rivera, and P. J. Sebastian, "Simulation of an air conditioning absorption refrigeration system in a cogeneration process combining a proton exchange membrane fuel cell," *Int. J. Hydrog. Energy*, vol. 32, pp. 3174–3182, 2007. https://doi.org/10.1016/j.ijhydene.2006.03.016.

[11] J. J. Hwang and M. L. Zou, "Development of a proton exchange membrane fuel cell cogeneration system," *J. Power Sources*, vol. 195, no. 8, pp. 2579–2585, 2010. https://doi.org/10.1016/j.jpowsour.2009.10.087.

[12] D. K. Madheswaran, A. Jayakumar, and E. G. Varuvel, "Recent advancement on thermal management strategies in PEM fuel cell stack: a technical assessment from the context of fuel cell electric vehicle application," *Energy Sources, Part A: Recover. Utiliz. Environ. Effects*, vol. 44, no. 2, pp. 3100–3125, 2022. https://doi.org/10.1080/15567036.2022.2058122.

[13] "High-performance polymer electrolyte membranes incorporated with 2D silica nanosheets in high-temperature proton exchange membrane fuel cells," *J. Energy Chem.*, vol. 64, pp. 323–334, 2022. https://doi.org/10.1016/j.jechem.2021.08.024.

[14] "Advances in polybenzimidazole based membranes for fuel cell applications that overcome Nafion membranes constraints," *Polymer*, vol. 255, p. 125151, 2022. https://doi.org/10.1016/j.polymer.2022.125151.

[15] "A Comprehensive Review of Stainless-Steel Bipolar Plate Coatings and Their Role in Mitigating Corrosion in Aggressive Proton-Exchange Membrane Fuel Cells Environments," *Chem. Eng. J.*, vol. 493, p. 152662, 2024. https://doi.org/10.1016/j.cej.2024.152662.

[16] H. Zhu, H. Chen, M. Zhang, C. Liang, and L. Duan, "Recent advances in promoting dry reforming of methane using nickel-based catalysts," *Catal. Sci. Technol.*, vol. 14, pp. 1712–1729, 2024. https://doi.org/10.1039/D3CY01612A.

[17] Y. Wang, Y. Zhao, G. Li, and G. Zhang, "Recent advances in Ni-based catalysts for $CH_4$-$CO_2$ reforming (2013–2023)," *Atmosphere*, vol. 14, no. 9, p. 1323, 2023. https://doi.org/10.3390/atmos14091323.

[18] J. Chen, J. Han, and D. Xu, "Efficient operation of autothermal microchannel reactors for the production of hydrogen by steam methane reforming," *Int. J. Hydrog. Energy*, vol. 44, no. 23, pp. 11546–11563, 2019. https://doi.org/10.1016/j.ijhydene.2019.03.025.

[19] S. Safari and H. A. Ozgoli, "Electrochemical modeling and techno-economic analysis of solid oxide fuel cell for residential applications," *J. Renew. Energy Environ.*, vol. 7, no. 1, pp. 40–50, 2020. https://doi.org/10.30501/jree.2020.105451.

[20] D. E. Garrett, *Chemical Engineering Economics*. New York, NY, USA: Van Nostrand Reinhold, 1989.

[21] K. T. Ulrich and S. D. Eppinger, *Product Design and Development*, 2nd ed. New York, NY, USA: McGraw-Hill, 2000.

[22] W. D. Seider, D. R. Lewin, and J. D. Seader, *Product and Process Design Principles: Synthesis, Analysis, and Evaluation*, 2nd ed. Hoboken, NJ, USA: John Wiley & Sons, 2004.

[23] A. Al Assadi, D. Goes, S. Baazouzi, M. Staudacher, P. Malczyk, W. Kraus, et al., "Challenges and prospects of automated disassembly of fuel cells for a circular economy," *Resour. Conserv. Recycl. Adv.*, vol. 19, p. 200172, 2023. https://doi.org/10.1016/j.rcradv.2023.200172.

[24] S. T. Thompson and D. Papageorgopoulos, "Platinum group metal-free catalysts boost cost competitiveness of fuel cell vehicles," *Nat. Catal.*, vol. 2, no. 6, pp. 558–561, 2019. https://doi.org/10.1038/s41929-019-0291-x.

[25] E. B. Agyekum, J. D. Ampah, T. Wilberforce, S. Afrane, and C. Nutakor, "Research progress, trends, and current state of development on PEMFC—new insights from a bibliometric analysis and characteristics of two decades of research output," *Membranes*, vol. 12, no. 11, p. 1103, 2022. https://doi.org/10.3390/membranes12111103.

[26] J. Cui, Q. Chen, X. Li, and S. Zhang, "Recent advances in non-precious metal electrocatalysts for oxygen reduction in acidic media and PEMFCs: an activity, stability, and mechanism study," *Green Chem.*, vol. 23, no. 18, pp. 7373–7404, 2021. https://doi.org/10.1039/D1GC01040A.

[27] S. Hosseinpour, S. A. H. M. Hosseini, R. Mehdipour, A. H. Hemmasi, and H. A. Ozgoli, "Energy modeling and techno-economic analysis of a biomass gasification-CHAT-ST power cycle for sustainable approaches in modern electricity grids," *J. Renew. Energy Environ.*, vol. 7, no. 2, pp. 43–51, 2020. https://doi.org/10.30501/jree.2020.106780.

[28] A. Arsalis, "Thermoeconomic modeling and parametric study of hybrid SOFC-gas turbine-steam turbine power plants ranging from 1.5 to 10 MWe," *J. Power Sources*, vol. 181, no. 2, pp. 313–326, 2008. https://doi.org/10.1016/j.jpowsour.2007.11.066.

[29] D. Cheddie and R. J. Murray, "Thermo-economic modeling of a solid oxide fuel cell/gas turbine power plant with semi-direct coupling and anode recycling," *Int. J. Hydrog. Energy*, vol. 35, no. 20, pp. 11208–11215, 2010. https://doi.org/10.1016/j.ijhydene.2010.07.084.

[30] R. S. Kempegowda, K. Q. Tran, and Ø. Skreiberg, "Economic analysis of combined cycle biomass gasification fuelled SOFC systems," *Int. Conf. Future Environ. Energy*, pp. 134–141, 2011.

[31] R. F. Boehm, *Design Analysis of Thermal Systems*. Hoboken, NJ, USA: Wiley, 1987.

[32] International Energy Agency (IEA), *World Energy Outlook 2023*. Paris, France: IEA, 2023. Accessed: Jul. 2, 2024. [Online]. Available: https://www.iea.org/reports/world-energy-outlook-2023.

[33] Eurostat, *In 2022, Energy Consumption in the EU Decreased by 5.9%*. Luxembourg: Eurostat, 2023. Accessed: Jul. 26, 2023. [Online]. Available: https://ec.europa.eu/eurostat/web/products-eurostat-news/w/ddn-20231026-1.

[34] Asimptote Software, "Cycle-Tempo details [Internet]," Accessed: Jun. 12, 2024. [Online]. Available: http://www.asimptote.nl/software/cycle-tempo/cycle-tempo-details.

[35] S. Chugh, C. Chaudhari, K. Sonkar, A. Sharma, G. S. Kapur, and S. S. Ramakumar, "Experimental and modelling studies of low-temperature PEMFC performance," *Int. J. Hydrog. Energy*, vol. 45, no. 15, pp. 8866–8874, 2020. https://doi.org/10.1016/j.ijhydene.2020.01.019.

[36] K. Subin and P. K. Jithesh, "Experimental study on self-humidified operation in PEM fuel cells," *Sustain. Energy Technol. Assess.*, vol. 27, pp. 17–22, 2018. https://doi.org/10.1016/j.seta.2018.03.004.

[37] H. F. M. Mohamed, E. E. Abdel-Hady, M. M. Abdel-Moneim, "Proton conductivity and free volume properties in per-fluorinated sulfonic acid/PTFE copolymer for fuel cell," *Acta Physica Polonica A*, vol. 132, no. 5, pp. 1509–1514, 2017. https://doi.org/10.12693/APhysPolA.132.1509.

[38] H. F. Mohamed, E. E. Abdel-Hady, M. M. Abdel-Moneim, M. A. Bakr, M. A. Soliman, M. G. Shehata, et al., "Effect of $Al_2O_3$ on nanostructure and ion transport properties of PVA/PEG/SSA polymer electrolyte membrane," *Polymers*, vol. 14, no. 19, p. 4029, 2022. https://doi.org/10.3390/polym14194029.

[39] M. Grandi, S. Rohde, D. J. Liu, B. Gollas, and V. Hacker, "Recent advancements in high-performance polymer electrolyte fuel cell electrode fabrication—Novel materials and manufacturing processes," *J. Power Sources*, vol. 562, p. 232734, 2023. https://doi.org/10.1016/j.jpowsour.2023.232734.

[40] S. Rogalsky, J. F. Bardeau, S. Makhno, O. Tarasyuk, N. Babkina, T. Cherniavska, et al., "New polymer electrolyte membrane for medium-temperature fuel cell applications based on cross-linked polyimide Matrimid and hydrophobic protic ionic liquid," *Mater. Today Chem.*, vol. 20, p. 100453, 2021. https://doi.org/10.1016/j.mtchem.2021.100453.

[41] Y. Lee, Y. Kim, J. C. Kim, and J. T. Chung, "Performance characteristics of a polymer electrolyte fuel cell with the anodic supply mode," *J. Power Sources*, vol. 160, no. 1, pp. 282–289, 2006. https://doi.org/10.1016/j.jpowsour.2006.02.033.